Deep learning-based synthetic CT from black-bone MRI with limited retrospective clinical data for MR-only treatment planning

Merlin Owens[1,2]; N. Jane Taylor, PhD[1]; Anwar Padhani, MBBS[1]; Andrew King, PhD[2]
[1]Paul Strickland Scanner Centre, [2]King's College London

2026 JULY 19–22 VANCOUVER, BC
JOINT AAPM | COMP MEETING

ABSTRACT

Purpose: To assess 'black-bone' MRI (inverted PD contrast spoiled-GRE) as an input to synthetic CT algorithms.

Methods: 5-fold cross validated U-Nets were trained on black bone and T1 Dixon in-phase inputs. Image metrics were compared, included bone- and soft tissue-specific MAE. A comparative radiotherapy plan was made.

Results: Black-bone and T1 Dixon in-phase trained networks produced a bone-specific MAE of 317.5 ± 35.0 HU, and 431.8 ± 53.4, respectively.

Conclusion: Black-bone trained networks were shown to produce a statistically significant reduction in the error for cortical bone estimation compared to T1 Dixon in-phase models.

CONTACT

Merlin Owens
Paul Strickland Scanner Centre,
Northwood, HA6 2RN, England
merlin.owens@nhs.net

INTRODUCTION

Bone estimation is challenging in synthetic CT due to poor bone contrast in standard MRI, due to the ultrashort T2 decay times of cortical bone. Black-bone MRI has been shown to provide excellent contrast of the cortical bone compared to standard MRI sequences [1]. Black-bone has a strong resemblance to CT on contrast inversion. Synthetic CT literature often explores new deep learning (DL) models used for synthetic CT generation but rarely discusses the effect of sequence on model training and the accuracy of the resulting synthetic CT[2,3]. Synthetic CT literature often uses T1 [4], T2[5], quantitative maps[6], ZTE[7,8,9], and UTE [10] inputs, but has yet to use black-bone as an input sequence.

We aimed to evaluate whether this improved cortical bone contrast could be exploited as an input to deep-learning based synthetic-CT models for the improved estimation of the Hounsfield units of cortical bone in the resulting synthetic CT. This could then be used for improved accuracy in MR-only treatment planning.

METHODS AND MATERIALS

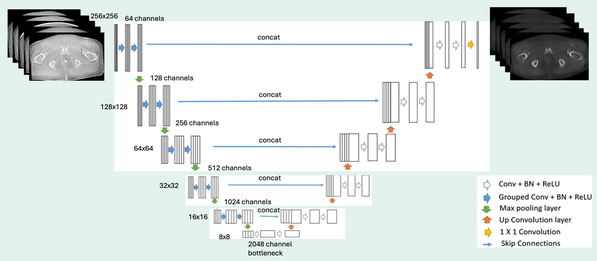

Figure 1. U-Net architecture used in training. Figure adapted from [11].

- Acquisition: black-bone MRI (TE=4.77ms, TR=6.4ms, FA=3°)/T1 Dixon in-phase (T1Din) (TE=4.77ms, TR=6.83ms, FA=15°)
- Registered to CT using SimpleITK algorithm performing a two-stage rigid and affine transformation
- The contrast of the black-bone MRI was inverted
- N=15 paired datasets were split at the patient-level for 5-fold cross validation (CV)
- 10-2-3 train, validate, test
- Splits were consistent for training both models
- U-Net models trained with OneCycleLR [12] (learning-rate=3×10−43×10−4, batch-size=2) for 35 epochs, optimised with Adam [13], using a combined loss function ($\lambda_1 = 1.0$, $\lambda_2 = 0.1$)
- Mean absolute error (MAE), structural similarity index (SSIM), and peak signal-to-noise were reported, along with soft tissue and bone specific results by creating bone and soft tissue masks
- Paired t-tests compared results
- A comparative radiotherapy plan was created

$$L_{L1}(y,\hat{y}) = \frac{1}{N}\sum_i |y_i - \hat{y}_i|$$

$$L_{MSE}(y,\hat{y}) = \frac{1}{N}\sum_i (y_i - \hat{y}_i)^2$$

$$L = \lambda_{L1} L_{L1} + \lambda_{MSE} L_{MSE}$$

Figure 2. Combined loss functions.

	MAE (HU)	PSNR	SSIM (dB)	Bone MAE (HU)	Soft tissue MAE (HU)
Black-bone	81.9 ± 12.9	0.758 ± 0.029	26.55 ± 0.45	317.5 ± 35.0	66.4 ± 8.3
T1 Dixon in-phase	79.7 ± 16.9	0.768 ± 0.021	24.89 ± 0.65	431.8 ± 53.4	56.5 ± 7.5
Difference	**2.2 ± 4.0**	**0.01 ± 0.008**	**1.66 ± 0.20**	**114.3 ± 18.4**	**9.9 ± 0.8**

Table 1. Image metrics comparison results

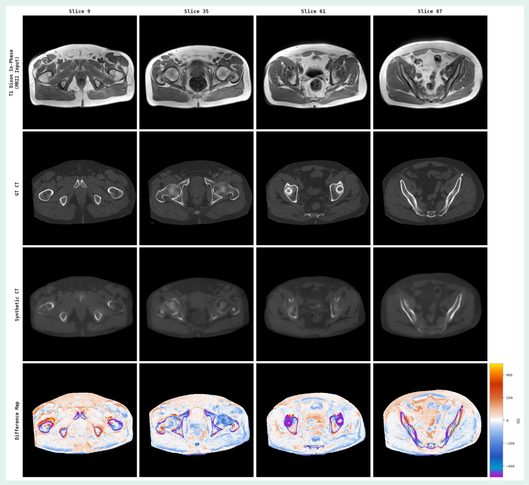

Figure 3. T1 Dixon in-phase sCT comparison grid.

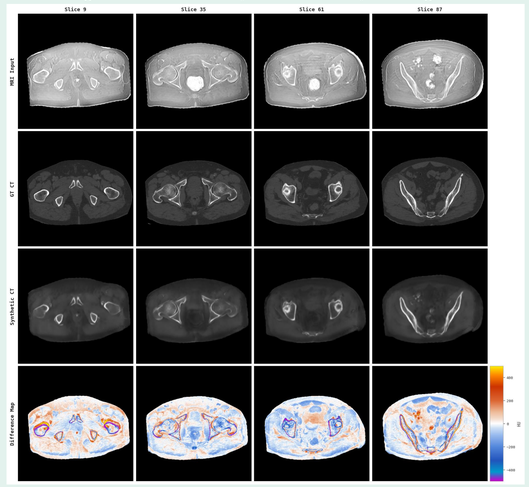

Figure 4. Black-bone sCT comparison grid.

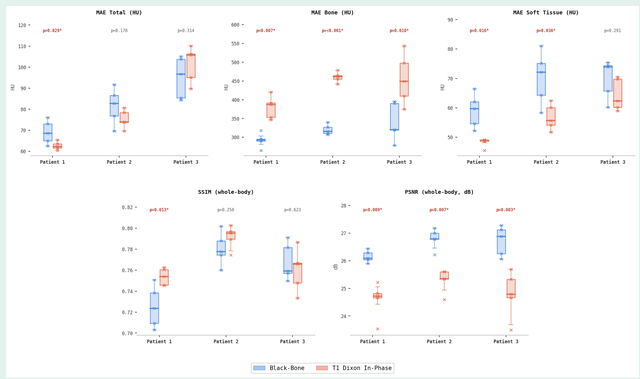

Figure 5. Box plots for each metric for each of the 3 test patients

RESULTS

MAE, PSNR, SSIM, Bone MAE, and soft tissue MAE averaged over all CV folds can be seen in Table. 1. Comparison grids showing the MR inputs, ground truth (GT) CT, synthetic CT, and difference map, across 4 slice positions for an example test patient, can be seen in Fig. 3 and Fig. 4. Box plots for each image metric for each test patient can be seen in Fig. 5. A comparative RT plan was created and had a dose difference to the PTV of 0.3%.

DISCUSSION

- With identically trained networks, black-bone MRI outperformed T1 Dixon in-phase inputs for CT bone generation in every test patient ($p<0.01$).
- Bone was better defined in BB MRI sCTs
- T1 Dixon in-phase had a statistically significant improvement in soft tissue, but this is minor overall (9.9 ± 0.8 HU)
- Misregistration, different couch shapes, patient setup differences, input sequence parameter differences are all limitations.

Future work:

- Standardised data acquisition in the planning position
- Explore other body regions for model training
- Dosimetric assessment
- Geometric assessment

CONCLUSIONS

Black-bone MRI was shown to be an effective input to deep learning based synthetic CT models, and produced a statistically significant improvement in the estimation of cortical bone, compared to the gold standard single input, T1 Dixon in-phase images. This was shown by training identical 5-fold cross validated networks for BB and T1 Dixon in-phase images.

This could improve accuracy in MR-only treatment planning, especially in sites treating around bone. Further study into the potential dosimetric improvements is needed.

REFERENCES

1. Eley, K.A. et al. (2012) '"black bone" MRI: A partial flip angle technique for radiation reduction in Craniofacial Imaging', The British Journal of Radiology, 85(1011), pp. 272–278. doi:10.1259/bjr/95110289.
2. Antunes Jacob, Young Tony, Pittock Dane, et al. Assessing multiple MRI sequences in deep learning-based synthetic CT generation for MR-only radiation therapy of head and neck cancers. Radiotherapy and Oncology. 2025;205:110782.
3. Qi Mengke, Li Yongbao, Wu Aiqian, et al. Multi-sequence MR image-based synthetic CT generation using a generative adversarial network for head and neck MRI-only radiother- apy. Medical Physics. 2020;47(4):1880-1894.
4. Han, X. (2017) 'MR-based synthetic CT generation using a deep convolutional neural network method', Medical Physics, 44(4), pp. 1408–1419. doi:10.1002/mp.12155.
5. Wang, Y. et al. (2019) 'Synthetic CT generation based on T2 weighted MRI of nasopharyngeal carcinoma (NPC) using a deep convolutional neural network (DCNN)', Frontiers in Oncology, 9. doi:10.3389/fonc.2019.01333.
6. Simkó, A. et al. (2024) 'Towards mr contrast independent synthetic CT generation', Zeitschrift für Medizinische Physik, 34(2), pp. 270–277. doi:10.1016/j.zemedi.2023.07.001.
7. Leynes, A.P. et al. (2017) 'Zero-echo-time and Dixon Deep Pseudo-ct (Zedd CT): Direct generation of Pseudo-CT images for pelvic pet/MRI attenuation correction using deep convolutional neural networks with Multiparametric MRI', Journal of Nuclear Medicine, 59(5), pp. 852–858. doi:10.2967/jnumed.117.198051.
8. Getzmann, J.M. et al. (2024) 'Deep learning-based pseudo-CT synthesis from Zero Echo time mr sequences of the pelvis', Insights into Imaging, 15(1). doi:10.1186/s13244-024-01751-3.
9. Weiger, M., Pruessmann, K.P. and Hennel, F. (2011) 'MRI with Zero echo time: Hard versus sweep pulse excitation', Magnetic Resonance in Medicine, 66(2), pp. 379–389. doi:10.1002/mrm.22799.
10. Jerban, S. et al. (2020) 'An update in qualitative imaging of bone using ultrashort echo time magnetic resonance', Frontiers in Endocrinology, 11. doi:10.3389/fendo.2020.555756.
11. Raju, C.S. et al. (2024) 'Analysis of Multimodal Fusion Strategies in deep learning for ischemic stroke lesion segmentation on computed tomography perfusion data', Multimedia Tools and Applications, 84(10), pp. 7493–7518. doi:10.1007/s11042-024-19252-2.
12. Al-Kababji Ayman, Bensaali Faycal, Dakua Sarada Prasad. Scheduling Techniques for Liver Segmentation: ReduceLRonPlateau Vs OneCycleLR. 2022.
13. Goodfellow, I., Bengio, Y. and Courville, A. (2017) Deep learning. Cambridge, MA: The MIT Press.